ISPRS Journal of Photogrammetry and Remote Sensing 144 (2018) 268–284

Contents lists available at ScienceDirect

ISPRS Journal of Photogrammetry and Remote Sensing

journal homepage: www.elsevier.com/locate/isprsjprs

Methods for quantification of systematic distance deviations under incidence angle with scanning total stations

Miriam Zámečníková*, Hans Neuner

Technische Universität Wien, Department of Geodesy and Geoinformation, Gußhausstraße 27-29, 1040 Wien, Austria

ARTICLE INFO

Keywords:
Systematic distance deviations
Reflectorless distance measurement
Incidence angle
Scanning total station

ABSTRACT

If scanning total stations (TLS + TS) are used in scanning mode for high accurate engineering applications, the systematic influence of the incidence angle (IA) on the reflectorless distance measurement has to be eliminated. At present, methods for quantifying the systematic distance deviations under IA are missing because the measured points are not reproducible. In this paper, three such methods are presented. They are conditional on the used instruments and the required accuracy. These methods are validated with respect to specified framework conditions. The distance deviations are derived in all three methods as difference between the distance measured with TLS + TS in the scanning mode (D_{TLS}) and the corresponding reference distance (D_{ref}). The D_{ref} is determined in three steps: measurement of a high accuracy network, measurement for determining the starting point of the D_{ref}; object measurement to determine the endpoints of D_{ref}. The corresponding D_{TLS} and D_{ref} are identified by means of the horizontal direction Hz (Hz_{TLS} and Hz_{ref}) and the vertical angle V (V_{TLS} and V_{ref}), both pairs of angles referring to the same origin marked by the axis of the common coordinate system. Depending on the used method, the D_{ref} is determined with a standard uncertainty of 0.1–0.3 mm (at a distance of 30 m). The quantified influence of IA on the distance measurement of the Leica MS50 at a distance of 30 m to a granite plate varies in the interval of 0.8 mm. The strong variation due to the IA occurs from 0 to 20 gon, its effect is stable from 20 to 60 gon.

1. Introduction

If known and unknown influences affect measured quantities, systematic measurement deviations can occur. They bias measurement data, such that they deviate from true values (Niemeier, 2008, pp. 10–12). In order to eliminate them, the measurement process has to be analyzed, influences have to be investigated and their correlations determined. Thereafter, they can be compensated by appropriate measurement strategies (by averaging or differentiating), by applying corrections determined in the calibration, or by implementing the systematic parameter as unknown in evaluation models. The elimination of the systematic deviations is essential for exploiting the accuracy potential of measuring instruments.

The scan data (point cloud) measured by terrestrial laser scanners (TLS) are influenced by instrumental imperfections, atmospheric effects, scanning geometry, object properties or surface related effects and georeferencing, e.g. (Soudarissanane et al., 2011; Boehler et al., 2003; Zogg, 2008, pp. 49–75; Ge, 2016, pp. 63–90). These error sources are partially investigated in the component calibration (Dorninger et al., 2008; Zámečníková et al., 2014b; Schulz, 2007, pp. 23–72) and estimated in the functional model of the system calibration (Lichti, 2007; Lichti et al., 2011; Gordon, 2008, pp. 50–57; Reshetyuk, 2009, pp. 66–114; Holst and Kuhlmann, 2014). The quantified calibration parameters are usually related to the frame conditions of the study. The properties are not generalized and no generally valid complete models are set up. It is caused by the specific design of each TLS as a black box that evokes other systematic errors, by the variety of combinations of scanning geometry and object properties (e.g. radiometric properties) and other behavior of each scanner to the complexity of the measurement conditions.

The non-considered systematic deviations of the measured data can lead to feigning rigid body movements, feigning object deformations or a combination of both. In order to use the TLS for measurements with an accuracy level of 1–2 mm (documentation, deformation monitoring it is necessary to develop the strategies for the elimination of the systematic deviations (Holst and Kuhlmann, 2014; Eling, 2009, p. 99; Wang, 2013, p. 52; Sarti et al., 2009).

The mentioned influence of the scanning geometry includes the IA of the laser beam. The IA is defined as the angle between the measuring beam and the normal to the plane, which locally approximates the

* Corresponding author.
E-mail address: miriam.zamecnikova@geo.tuwien.ac.at (M. Zámečníková).

https://doi.org/10.1016/j.isprsjprs.2018.07.008
Received 22 January 2018; Received in revised form 8 July 2018; Accepted 17 July 2018

measured area during the scanning process. The laser beam falls on surfaces of different orientation, i.e. the IA changes. The variation of the IA causes systematic distance deviations, e.g. (Zámečníková et al., 2015; Zámečníková and Neuner, 2017a, 2017b).

The measurement deviations due to the influence of IA are explained in two ways in the geodetic expert group. In a first way, the laser footprint is deformed by the resulting geometry. Under IA are different distances in the beam path, which are within a certain distance interval, which depends on the size of the beam diameter on the surface and the orientation of the surface (Jutzi, 2007, p. 13). Thus, the center point of the laser spot does not coincide with the endpoint of the distance. Furthermore, the average value of the distances within the laser spot is longer than the distance corresponding to the measured horizontal direction and vertical angle (Schulz, 2007; Gordon, 2008, pp. 30–31; Linstaedt et al., 2009). In the second way, under higher IA, the reflected signal strength is reduced (Schäfer and Schulz, 2005; Kersten at al., 2008; Wujanz et al., 2017). The intensity of the reflected signal strength in the nearer part of the laser spot dominates in the measurement signal and leads to shorter distances (Kern, 2003, p. 41–42; Joeckel et al., 2008, pp. 10–12; Schäfer, 2017, pp. 78–81). There is no weighting process in signal processing yet the parts of the signal have a higher impact onto the distance. According to previous explanations, the distances with increasing IA may become shorter or longer.

The distance deviations could be investigated at the level of the received signal strength (radiometric level) or/and at the distance level. Outgoing from the known received signal strength, a model for the transfer of the received signal strength to the distance under IA is missing. Also, the transmitted and received waveform is not present over time, so the approach for airborne laser scanner (Roncat, 2014, pp. 10–26; Jutzi, 2007, pp. 32–48) cannot be applied. Basically, if the investigation existed on the radiometric or/and distance level, the validation of the approach would be necessary also on the distance level. In this paper, the systematic distance deviations are investigated only on the distance level.

A general problem makes the quantification of the systematic distance deviations due to the influence of the IA in the scanning mode more difficult. The endpoints of the measured distances are not signalized and reproducible. In Mechelke et al. (2007) a plane under IA is scanned with four spheres as reference points. The variation of the distance offset between the approximated plane through the point clouds and center points of approximated reference points respectively was observed and set as a measure for the effect of the IA. If the geometry of the measuring object deviates, the influence of the IA is not correctly quantified by the indirect derivation (Wujanz et al., 2017). Typically, this influence is not included in the functional model of the measured distance for a system calibration (Lichti, 2007; Lichti et al., 2011; Gordon, 2008, pp. 50–57; Reshetyuk, 2009, pp. 66–114; Holst and Kuhlmann, 2014). In order to tackle this influence, methods for its quantification are required.

The aim of the paper is to introduce novel metrological methodologies, which are focused on the direct comparison of distances measured in scanning mode under laboratory condition with reference distances in order to assess the influence of the IA. Three methods for quantification of the systematic deviations under IA are presented, validated and critically compared. Two of the methods were partly published in the context of different research questions (Zámečníková et al., 2015; Zámečníková and Neuner, 2017a, 2017b). They serve as a developed tool that research institutions can use.

Currently, the methods are suitable for scanning total stations (TLS + TS) operated in scanning mode, as they use the total station part of TLS + TS. The use of TLS + TS constitutes a bridging solution towards applicability for usual TLS. The methods are based on individually measured distances, i.e. circumventing indirect derivation by the modeling of the measured object (Wujanz et al., 2017). The application of these methods is given by the available instruments and by the required accuracy of the reference distance.

The proposed methodological approach is regarded as one step forward towards the complex investigation of the scanning geometry on the reflectorless distance measurement. The quantified systematic distance deviations contribute to the understanding of the influences and enable to select their compensation strategy, e.g. the derivation of the term for the functional model of the measured distances in the system calibration.

The paper is structured as follows: in the second chapter, the concepts common to all three methods for the quantification of systematic distance deviations under IA are introduced. In the 3rd chapter the framework conditions of the experiments are given for all methods, the measuring setup, the measurement process and the evaluation of each method are described. In the 4th chapter, the results of all experiments are shown and analyzed for validation of the methods. Finally, the paper is summarized and an outlook is given.

2. Methodology

The quantification of the systematic distance deviations is based in all three methods on the comparison of the distance measured by a total station in the scanning mode (D_{TLS}) with the corresponding reference distance (D_{ref}) (Fig. 1).

2.1. Reflectorless distance D_{TLS}

The investigated reflectorless distance D_{TLS} is defined by the distance between the zero point of the TLS + TS (P_0) and the object point (P) under measured Hz_{TLS}, V_{TLS} (Fig. 1).

As the measurement result of TLS + TS, the rectangular coordinates of the measured point cloud (y_{TLS}, x_{TLS}, z_{TLS}) refer to the TLS + TS coordinate system (CS). Its origin is located in P_0, the x-axis corresponds to the zero direction of the Hz-circle and the z-axis to the vertical axis of the instrument. It is assumed that the polar elements Hz_{TLS}, V_{TLS}, D_{TLS} calculated from the obtained rectangular coordinates correspond to the measured ones. Furthermore, it is assumed that in case of the TLS + TS the angles of the scanner component (Hz_{TLS}, V_{TLS}) and of the total station component (Hz_{TS}, V_{TS}) are equal ($Hz_{TLS} = Hz_{TS}$, $V_{TLS} = V_{TS}$).

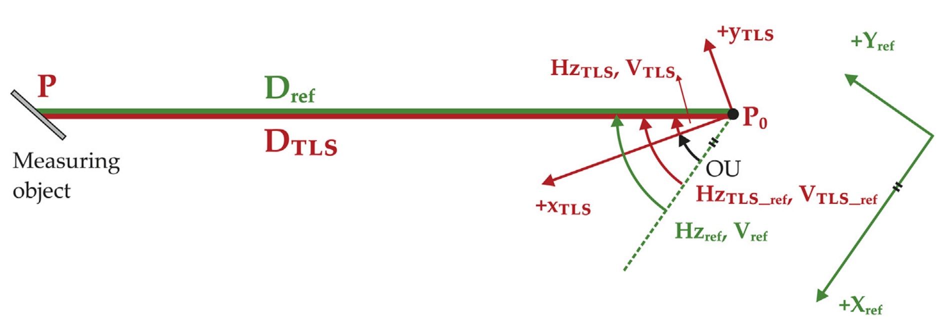

Fig. 1. The common principle of the three methods.

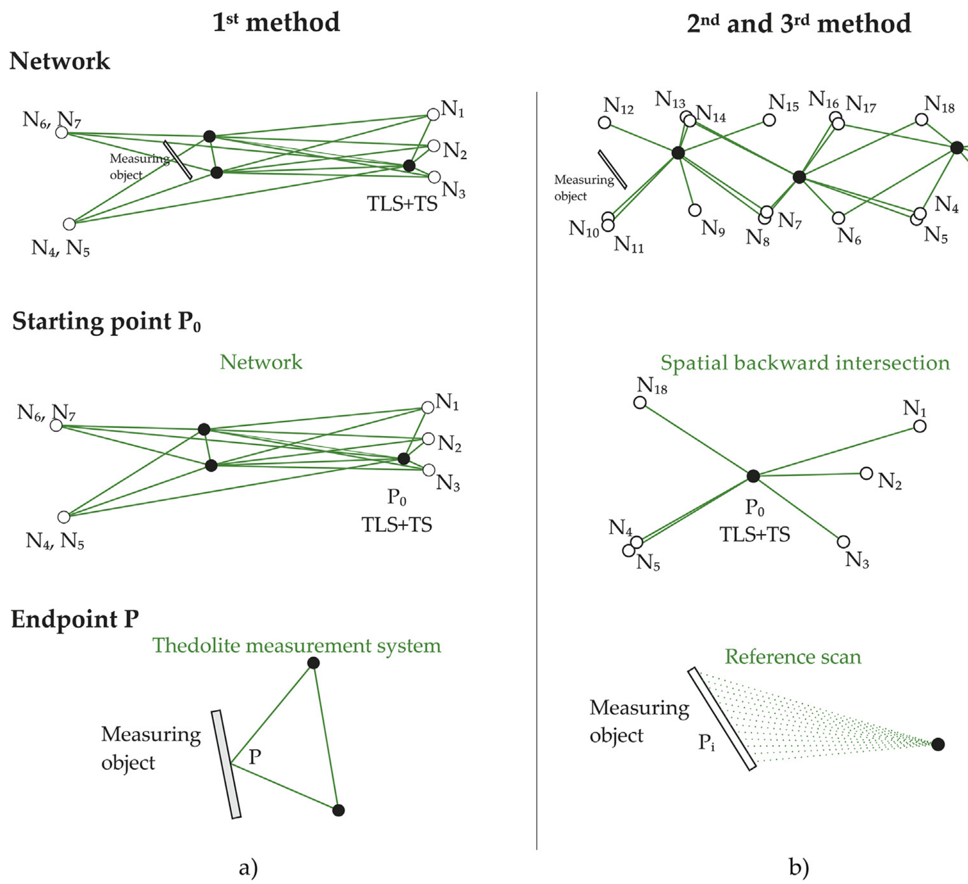

Fig. 2. Determination of D_{ref} in the (a) 1st method, (b) 2nd and 3rd method.

2.2. Reference distance D_{ref}

The reference distance D_{ref} corresponding to the D_{TLS} is determined with one order of lower uncertainty than the uncertainty of the examined D_{TLS}. D_{ref} is determined in three steps (Fig. 2):

(1) Determination of a high accuracy network, which extends over the investigated distance,
(2) Determination of P_0 as part of the network (1st method) or by a spatial backward intersection (SBI) from network points (2nd and 3rd method),
(3) Determination of P by point-wise (1st method) or by area-wise measurement techniques (2nd and 3rd method) with reference to the network points.

The reference distance is calculated from the coordinates of P_0 and P (Fig. 1)

$$D_{ref\_i} = \sqrt{(Y_{ref\_Pi}-Y_{ref\_P0})^2 + (X_{ref\_Pi}-X_{ref\_P0})^2 + (Z_{ref\_Pi}-Z_{ref\_P0})^2}. \tag{1}$$

A prerequisite for plausible derivation of the D_{ref} is the stability of the measuring setup. For stability check, repeated observations are compared during the entire investigation to the first observations. The difference between these observations was assessed by the test of the difference between two uncorrelated measured values with a significance level of $\alpha = 5\%$, two side-alternative hypothesis (Heunecke et al., 2013, p. 158 ff.).

For each method, influences affecting the determination of the D_{ref} are analyzed and quantified. In terms of the relevant influences, the uncertainty of the D_{ref} was derived according to the Guide to the Expression of Uncertainty in Measurement (GUM) (JCGM 100:2008).

2.3. Pairs of the corresponding distances D_{TLS} and D_{ref}

Establishing correspondences between D_{ref} and D_{TLS} requires the identification of the endpoint P of the D_{TLS}, in order to determine the endpoint of D_{ref} (Fig. 1).

Two variants of this identification were developed (Fig. 3):

1. S-method (staking out) – the endpoint is staked out by means of Hz_{TLS}, V_{TLS} with the TS component of the TLS + TS and physically signalized. The endpoint is determined by the reference measurement (direct signalizing and reference determination).
2. N-method (nearest neighbour) – the object is captured by a very dense reference scan with superordinate uncertainty. This reference point cloud is related to the reference CS. Assuming that the TLS + TS point cloud is oriented to the reference CS, the directions Hz_{TLS}, V_{TLS} allocated to D_{TLS} can be expressed as Hz_{TLS_ref}, V_{TLS_ref} (see Fig. 3b)). Therefore, the endpoint of D_{ref} is determined as the nearest neighbor to Hz_{TLS_ref}, V_{TLS_ref} in the reference scan (area-wise reference determination without direct signalizing).

2.4. Distance deviations

From corresponding distances, the systematic distance deviations are expressed as:

$$\Delta D_i = D_{ref\_i}-D_{TLS\_i}. \tag{2}$$

For each alignment of the measuring object (1 IA) several distance deviations are determined. These are averaged in order to reduce the stochastic part of the determination:

$$\Delta D_m = \sum_{i=1}^{n} \frac{\Delta D_i}{n}. \tag{3}$$

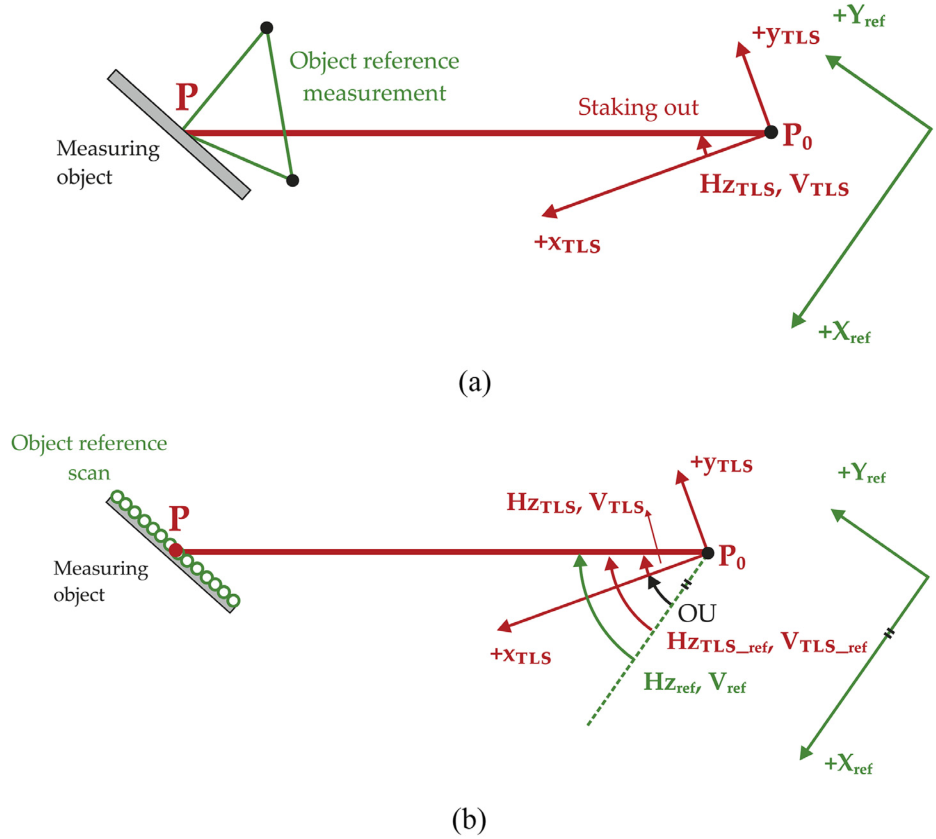

Fig. 3. Identification methods: (a) S-method and (b) N-method.

The standard deviation of the mean ΔD_m is:

$$\sigma_{\Delta Dm} = \sqrt{\frac{\sum_{i=1}^{n} (\Delta D_m - \Delta D_i)^2}{n(n-1)}}. \tag{4}$$

On the basis of the variation of ΔD_m and $\sigma_{\Delta Dm}$ with IA, the systematic character of the influence of the IA on the distance measurement is assessed.

2.5. Assessment of the influence of IA

The relevance of the distance variation under the influence of the IA was judged with the statistical test for two uncorrelated values with a significance level of $\alpha = 5\%$ (Heunecke et al., 2013, p. 158 ff.). The zero and alternative hypotheses are

$$H_0: E(d_i) = 0, \tag{5}$$

$$H_A: E(d_i) \neq 0, \tag{6}$$

where d_i is the difference of the distance deviations between two IA (j, k)

$$d_i = \Delta D_{IA\_k} - \Delta D_{IA\_j}. \tag{7}$$

3. Framework of investigation

The reflectorless distances measured under IA were examined with a TLS + TS Leica Nova MultiStation MS50 (MS50) (Surveyequipment, 2013), in one exceptional case with its successor Leica Nova MultiStation MS60 (MS60) (Leica Geosystems, 2015). The relevant technical parameters for the investigation are listed in Table 1. The measuring process was automated via Geocom interface.

The experiments were performed under laboratory conditions in order to ensure controllable atmospheric parameters and stability conditions. On the other hand, this limits the investigated distances to approx. 30 m. However, this distance is beyond the close range domain, where additional effects i.e. due to the overlapping of the transmitted and received signal can affect the measured distances. The distances D_{TLS} were measured in one face of the telescope, with the object resolution of 1 cm. The scanning frequency was set to the lowest possible value of 62 Hz. In case of (almost) planar surfaces like the analyzed one, it is a reasonable assumption that this setting minimizes the TLS noise.

With regard to the specified standard deviation of D_{TLS} (see Table 1), the D_{ref} should be determined with a standard deviation of 0.2 mm. When designing the experiments this requirement was interpreted tighter in terms of an aimed uncertainty of 0.2 mm.

The distances were measured to an approximately planar plate (Fig. 4). The chosen object has not more complex form to avoid significant different IA for one alignment of the object. However, no specific assumption on the entire object's geometry is made for the investigation.

The measuring object is from granite which is easily accessible. A possible disadvantage of this material can be the transmission effect of

Table 1
Technical parameters of MS50/MS60 (Surveyequipment, 2013; Leica Geosystems, 2015).

Technical parameter	Standard deviation (σ)
Angle measurement	0.3 mgon
Distance measurement with reflector	1 mm + 1.5 ppm
Distance measurement without reflector (reflectorless)	2 mm + 2 ppm
Scanning – range noise (measurement frequency of 62 Hz)	0.4 mm at 10 m 0.5 mm at 25 m
Laser dot size (elliptical)	Approx. 7 × 10 mm at 30 m

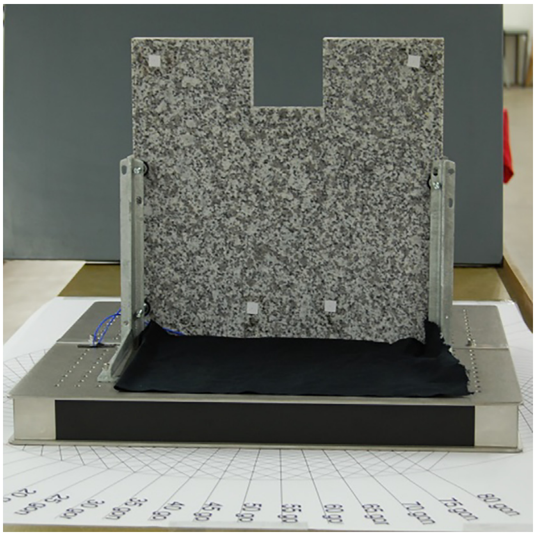

Fig. 4. Measuring object – granite plate.

the laser. This may influence the quantified distance deviations. Thus, for the comparison of the results it is important to use the same measuring object in the experiments. The surface of the plate is smooth in order to reduce the influence of the roughness to a large extent.

The plate is arranged nearly vertical in a stable stand, which consists of two holders (left, right) and a robust base plate (Thorlabs, 2018). The middle section of the plate with dimensions of $20 \times 10\,cm^2$ was scanned.

In order to set a specific IA, the base plate and the measuring object were rotated about an approximate vertical axis (horizontal part of the IA) with respect to a previously oriented angle scale. It is assumed that all distances measured to the plate at the same alignment setup are affected by the same influence of the IA. The maximal variation of IA at one object alignment is 0.5 gon ($IA = 0$ gon).

If the measuring object is rotated in the clockwise direction, the IA are positive, in the case of counterclockwise rotation, the IA are negative. The distances were measured at least under 10 IA - (0, 10, 20, 30, 35, 40, 45, 50, 55, 60) gon. The same set of positive and negative IA differs by max. 0.45 gon with respect to the used equipment.

It can be summarized, that the quantified ΔD reflect influences on D_{TLS} that vary with IA. Some of them are the IA itself (alignment of the measurement object with respect to the laser beam), surface properties (penetration depth, roughness as in Zámečníková and Neuner (2017a), etc.) and the influence of the instrument (the size of the laser spot).

3.1. First method

The idea of the first method comes from an investigation of the D_{TLS} in the close range (Zámečníková et al., 2014), whereby the high accuracy network extended the reference measurement. The endpoints of the D_{TLS} are staked out (S-identification method). Two experiments were carried out for this method (e1.1, e1.2). In the second experiment (e1.2), improvement suggestions from the e1.1 were implemented in the measuring arrangement and process as well. Therefore, the more developed e1.2 is described representative in this paper.

3.1.1. Measuring setup and process

The measuring setup of this method is shown in Fig. 5. The measuring object was positioned in the transverse middle area of the measuring laboratory. The TLS + TS stood on a pillar at a distance of 30 m from the measuring object. Two additional total stations TS_1 (Leica TM30) and TS_2 (Leica TS50) as a theodolite measurement system (TMS), both with an angular standard deviation of 0.15 mgon, distance standard deviation of 0.6 mm + 1 ppm (Leica Geosystems, 2009a; Surveyequipment, 2013)) were set up on the industrial tripod and wooden tripod in the object distance of about 2 m. The distance between these two stations was about 2.4 m, which represents a basis for spatial forward intersection (SFI). There were seven Leica round prisms (N_1–N_7) on consoles and pillars. All of these station points and prisms form a high accuracy network (length × width × height, $53 \times 6 \times 2\,m^3$). In order to define the scale of the network, the basis of the SFI is determined by Hansen's task (Kahmen, 2006, pp. 296–299). For this purpose, a reference scale with a length of approx. 0.87 m was positioned horizontally and its length was measured by the interferometer Agilent 5530, standard deviation of the reference scale 0.4 ppm (Agilent Technology, 2008).

In the experiment e1.1 two total stations were used with lower accuracy with angular standard deviation of 0.3 mgon, distance standard deviation to prisms of 2 mm + 2 ppm or 1 mm + 1.5 ppm (Leica Geosystems, 2009b; Geotech, 2006) and without a reference scale.

First, the measurement of the high accuracy network was performed. The measured quantities of horizontal directions (Hz), vertical angle (V), slope distances (D) were measured in three sets manually sighting from each station point (TLS + TS, TS_1, TS_2) to prism N_1-N_7. The Hz and V between station points were determined by collimation. After that, the base TS_1TS_2 was determined by Hansen's task. From TS_1 and TS_2, Hz and V were measured to the two points of the reference scale in three sets. In order to avoid centering errors, the instruments remained in the tripod during the whole investigation. The mutual collimation between TS_1 and TS_2 was performed before each object alignment (1 IA) to assert a possible twisting of the horizontal circle.

In e1.1 the network measurements were carried out with ATR, which is less accurate (Leica Geosystems, 2009b; Geotech, 2006) than the manually sighting for short distances.

Each alignment of the measuring object (each IA) was scanned by TLS + TS under the certain scan parameters. The point cloud results in the instrument coordinate system. From the scan (y_{TLS}, x_{TLS}, z_{TLS}), five random points (P_i) were selected to which the D_{TLS} was examined. The polar elements Hz_{TLS}, V_{TLS}, D_{TLS} were recalculated from the coordinates y_{TLS}, x_{TLS}, z_{TLS} of endpoint P_i and zero point P_0. As $Hz_{TLS} = Hz_{TS}$ and $V_{TLS} = V_{TS}$, a point P_i was staked out from TLS + TS in the first face of the telescope (same as in scanning mode) and was signalized with a needle (Fig. 6). Subsequently, the Hz and V were measured to the signalized point in two faces of the telescope from station points of TS_1 and TS_2 (by TMS). The next points of a plate alignment were individually staked out and determined via TMS.

The possible instability of the measuring object as a result of staking out or leaning the needle on the measuring object has been checked. To this, four points located in corners of the measuring object were observed by means of SFI in two faces before and after the staking out of object points of one object alignment (1 IA).

The TLS + TS scanning, staking out, TMS-determination and control of the stability of the measuring object were carried out for each configured IA of the measuring object.

The stability of the station points over the time of the whole investigation was regularly checked by means of the network measurement in one set with ATR to the prisms N_1-N_7 and mutual collimation between station points. In e1.2, the base TS_1 and TS_2 were also determined repeatedly.

3.1.2. Post-processing

The D_{ref} corresponding to the measured D_{TLS}, whose endpoint was physically signalized according to the S-identification method, was derived in the following steps:

1. Determination of reference network points (TLS + TS, TS_1, TS_2, N_i) – Y_{ref}, X_{ref}, Z_{ref}

The network points were obtained by a free network adjustment (max. standard deviation of a coordinate of 0.03 mm) of all network

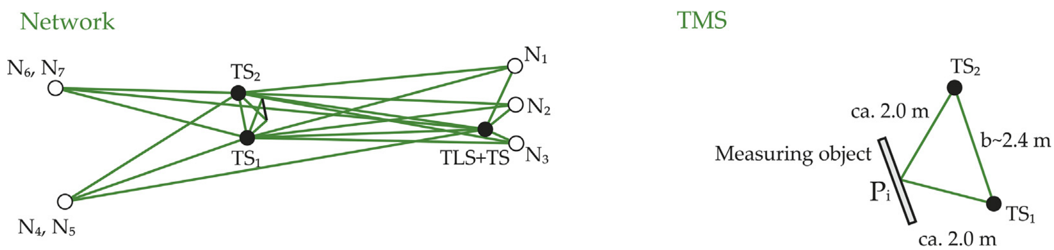

Fig. 5. Measuring setup of the first method - experiment e1.2 (pairs of network points N_4, N_5 and N_6, N_7 have nearly same 2D-position, but different heights).

Fig. 6. Signalizing the staked out point with a needle.

measurements and stability measurements with datum points TS_1, TS_2, TLS + TS. Actual instrumental parameters of the total stations were considered according to (ISO 17123-4, 2012).

For e1.2 the high accuracy horizontal distance D_{TS1TS2} flows into the network adjustment, which was determined by Hansen's task (standard deviation of 0.02 mm).

2. Reference determination of the object points (P_i) – Y_{ref_Pi}, X_{ref_Pi}, Z_{ref_Pi}.

Starting from the horizontal base TS_1 and TS_2, the object points P_i are calculated over the SFI (max. standard deviation of a coordinate 0.02 mm).

3. Determination of the reference distances D_{ref_i} by Eq. (1) and uncertainty evaluation

The influences on the determination of D_{ref} referring to e1.2 are listed in Table A1 and quantitatively assessed. The measuring setup of the station points is considered to be stable on the basis of repeated measurements despite some outliers. The uncertainty according to GUM of the mean D_{ref} (the average of five D_{ref} at an IA) is 0.25 mm, (Table A2).

3.2. Second method

The second method uses the modern instruments of higher accuracy - laser tracker (LT) and scanner arm with an attached triangulation scanner (SA + TS). The N-identification method of the object points results from the area-wise acquisition of the measuring object. The measuring process and the evaluation of this method are nearly identical to the third method (Section 3.3) because they are based on the same identification method. To avoid duplication, both parts are explained in more detail in the next section.

3.2.1. Measuring setup and process

Four LT nests for CCR reflectors (1.5″) (T_1–T_4) were attached to the measuring object and used as tie points. They were mounted at the edges of the granite plate (Fig. 7). The high accuracy network was also signalized with 13 nests (N_1–N_{13}). Two LT station points (LT_1, LT_2)

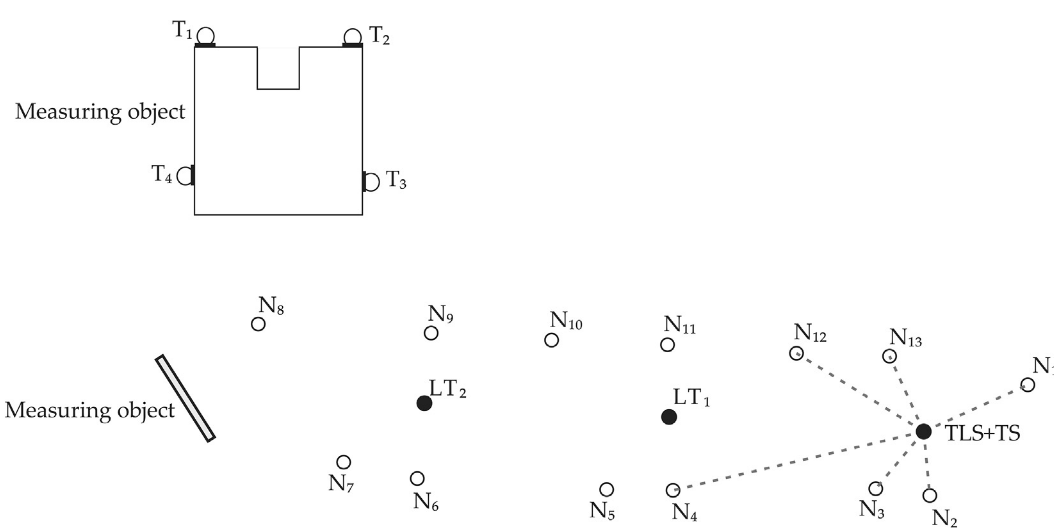

Fig. 7. Measuring setup of the second method.

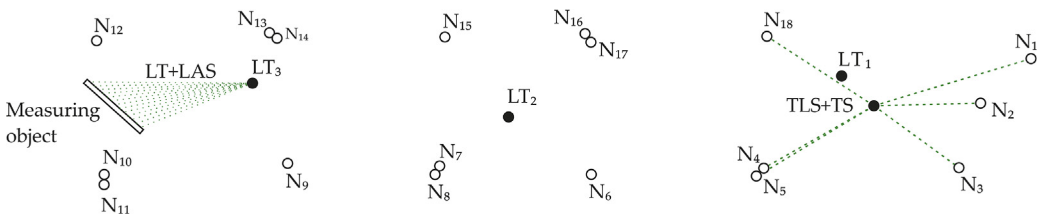

Fig. 8. Measuring setup of the third method.

were in the longitudinal axis of the network. The laser tracker Leica AT960 (max. allowable deviation (MPE) of 15 µm + 6 µm/m (Hexagon manufacturing intelligence, 2015)) was used for the network measurement. The TLS + TS was mounted on an industrial tripod at ca. 30 m from the measuring object. In addition to this measuring setup, the measuring object (up to 9 million points) and the tie points were captured by the scanner arm with an triangulation scanner Nikon Metrology (MMD50, 2σ = 16 µm (SouVR, 2017)).

In the measuring process, first the network measurement from two laser tracker station points was performed. Then, the Hz and V were measured by the TLS + TS to the respective network points. Further, the typical step for this method was realized. At each alignment the measuring object (1 IA) was scanned by TLS + TS as well as four tie points (T_1–T_4) of the measuring object were obtained by LT from the LT_2 position (measurement time of 3 s). During the investigation, the stability measurements of the measuring arrangement were carried out and finally the network was measured again.

In addition to the main measurement, the tie points on the measuring object (the CCR reflector positions) were measured by the stylus tip of the scanner arm and then the reflector center points were derived by the approximation. The coordinates refer to a local coordinate system of the SA. A reference scan of the measuring object was also captured with high point density by the triangulation scanner of the scanner arm.

3.2.2. Post-processing

The corresponding reference distances are derived as follows:

1. Determination of all D_{ref} (Hz_{ref}, V_{ref}) in the reference CS.

The network points as well as the four tie points (T_1–T_4) are transformed in the reference CS (max. standard deviation of a coordinate of 0.08 mm) per each alignment of the measuring object. The reference CS is defined by the inclination measurement of one LT station. The endpoints of the reference distances resp. the reference scan of each object was transferred to the reference CS via 6-parameter transformation (scale factor = 1) over four tie points (T_1–T_4) measured with the SA + TS and LT. The computations were performed using the geodetic toolbox for MATLAB; see (Mathworks, 2017). The starting point of the reference distances – the TLS + TS-zero point is determined by the SBI (max. standard deviation of a coordinate of 0.02 mm). The D_{ref} is calculated by equation (1).

2. Orientation of D_{TLS} (Hz_{TLS}, V_{TLS}) in the reference CS by a horizontal angle, i.e. the orientation unknown (standard deviation of 0.08 mgon) – (Hz_{TLS_ref}, V_{TLS_ref}).
3. Identification of the corresponding D_{ref} to D_{TLS} via Hz_{TLS_ref}, V_{TLS_ref} with the N-method (max. impact on the D_{ref} of 0.06 mm) and uncertainty evaluation.

The influences on the determination of the D_{ref} are listed in the Table B1. Repeated measurements by TLS + TS to the network points indicate the stability of TLS + TS, although some outliers are present. The uncertainty of the D_{ref} of 0.30 mm was derived by GUM (Table B2). The transformation of the reference point cloud over four tie points into the reference CS contributes to the higher uncertainty.

3.3. Third method

The third method provides a sophisticated approach for determining the investigated distance differences. Instead of the scanner arm with attached triangulation scanner used in the second method, a handheld scanner (HS) continuously tracked by the LT is employed. It enables the surface scanning directly in the CS of the LT. Its main advantage is that the need for a transformation by using tie points is omitted. On the other hand it is disadvantageous, as a reference scan must be captured at each alignment (1 IA) of the measuring object. The measuring setup, the measuring process and the post processing of three performed experiments e3.1-e3.3 are the same. The difference between e3.1 and e3.2 as well as e3.3 is that the measuring object has been rotated both clockwise (positive IA) and counter-clockwise (negative IA) about its approximately vertical axis. The last experiment e3.3 was performed independent from e3.2, after one week.

3.3.1. Measuring setup and process

The TLS + TS was positioned at about 30 m from the object on an industrial tripod (Fig. 8). The network consists of 18 points (N_1–N_{18}). They are signalized with nests for CCR reflector on the walls and floor. The network has dimensions of $36 \times 6 \times 3\,m^3$ (length × width × height). The points were measured from three station of LT AT960. The HS – Leica Absolute Scanner LAS-20-8 was tracked by the LT_3 (measurement uncertainty of room lengths (2σ) UL = 60 µm under 8.5 m (Hexagon Manufacturing Intelligence, 2018)).

The network was measured by the LT AT960 in two faces with measurement time of 5 s per point. In order to transfer the measured data into a horizontal reference CS, the inclination measurement of the LT-position was also carried out. In order to determine the zero point of the TLS + TS, Hz and V were measured by the TLS + TS to six nearby network points in three sets at the beginning and end of the investigation. The CCR reflectors need to be optimally aligned and illuminated. The measuring object was scanned by TLS + TS with the defined scan parameters and by HS with very high density (point density of 0.05 mm, up to 17 million points).

The stability of the TLS + TS and the LT_3 (in front of the measuring object) was monitored throughout the investigation by repeated measurement to the network points. In the end, the complete network measurement was performed.

3.3.2. Post-processing

The corresponding reference distances are derived in three steps:

1. Determination of D_{ref} (Hz_{ref}, V_{ref}) in the reference CS.

The coordinates of the network points and the reference point cloud were obtained by network adjustment with the function USMN (Unified Spatial Metrology Network) of the software Spatial Analyzer. The estimated network points (max. standard deviation of a coordinate of 0.06 mm) and the reference point clouds of the HS refer to the horizontal reference CS (Y_{ref}, X_{ref}, Z_{ref}) defined by the inclination measurement of LT-position LT_2. Then the starting point of the reference distances (the TLS + TS-zero point) is calculated by the SBI (max. standard deviation of a coordinate 0.02 mm). Finally, the polar elements D_{ref}, Hz_{ref}, V_{ref} are obtained from the reference rectangular coordinates (Y_{ref}, X_{ref}, Z_{ref}).

2. Orientation of D_{TLS} with respect to the reference CS → D_{TLS} (Hz_{TLS_ref}, V_{TLS_ref}).

The CS of the TLS + TS and the reference CS are horizontal oriented to gravity. Thus, $V_{TLS\_ref} = V_{TLS}$. The TLS + TS point cloud is oriented to the reference CS on the basis of a horizontal rotation angle - the orientation unknown (*OU*) (Hz_{TLS}, $V_{TLS} \rightarrow Hz_{TLS\_ref}$, V_{TLS_ref}) – the angle between the reference direction of both CS (Fig. 1). The *OU* (Fig. 1) equals the difference between the Hz calculated from the reference coordinates and the corresponding measured Hz to network points. The empirical standard deviation of the mean value is 0.07 mgon. The direction of the D_{TLS_i} is expressed in the reference CS:

$$Hz_{TLS\_i\_ref} = Hz_{TLS\_i} + OU. \tag{8}$$

3. Identification of the correspondent D_{ref} and D_{TLS} and uncertainty evaluation.

The directions of D_{ref} (Hz_{ref}, V_{ref}) and D_{TLS} (Hz_{TLS_ref}, V_{TLS_ref}) ideally have the same Hz-, V-reference direction. However, it cannot be assumed that the same object point is hit in the TLS and in the HS point cloud as well. Therefore, the correspondence between D_{ref_i} and D_{TLS_i} is fixed by the following nearest-neighbour approach:

$$Hz_{TLS\_i\_ref} - \Delta Hz \leqslant Hz_{ref\_i} \leqslant Hz_{TLS\_i\_ref} + \Delta Hz, \tag{9}$$

$$V_{TLS\_i\_ref} - \Delta V \leqslant V_{ref\_i} \leqslant V_{TLS\_i\_ref} + \Delta V. \tag{10}$$

ΔHz, ΔV denotes a permissible angle deviation from the exact value $Hz_{TLS\_i\_ref}$ and $V_{TLS\_i\_ref}$. It was determined in this study to be 0.1 mgon. In the worst case it causes a deviation of 0.06 mm from the D_{ref}. With this approach, 130–200 distances were identified per IA.

The influences, which can have a negative effect on the D_{ref} are summarized in the Table C1. The uncertainty of the D_{ref} according to GUM reached 0.09 mm (Table C2).

4. Validation

An overview of the differences as well as the specified details of the methods and experiments are given in Section 4.1. Possible influences on the investigated distance deviations originating the measuring process are explained in Section 4.2. Their consideration is described in Section 4.3. Finally, the Sections 4.4 and 4.5 introduce and comment on the obtained distance deviations respectively.

4.1. Overview of methods and experiments

The main features of the methods as well as differences between them are summarized in Table 2. The investigations were performed over two years, i.e. over the time of the development of more accurate method for the quantification.

The MS60 was used only in the experiment e3.1. Before the experiment e2.1 MS50 was maintained, while for e3.2 the reflectorless distance axis of MS50 was adjusted to the collimation axis by the manufacturer service.

Up to experiment 3.1, the object was measured only under negative IA of the laser beam. Starting with e3.2 the object is scanned under negative and positive IA in order to eliminate other effects that affect distance deviations under IA (Section 4.2).

For each experiment the parts of the reference determination, the requirement of the orientation of the TLS + TS-point cloud into the reference CS, the used method for the identification of the D_{TLS}-end point are given in Table 2.

4.2. Influences on the investigated distance deviations

The distance deviations obtained from (3) can be influenced by other instrumental errors and by error influences that come from the measuring process of the quantification methods. Some major influences causing distance deviations with increasing IA are analysed subsequently.

These influences affect either the D_{TLS} or the D_{ref} and are only present in certain methods:

1. Eccentricity between the distance axis and the collimation axis (influence on D_{TLS}, relevant for all methods)

The basic assumption used in the definition of D_{TLS} (Hz_{TLS}, V_{TLS}) is that the distance axis coincides with the collimation axis. If this assumption is incorrect an eccentricity occurs which is denoted by ε in Fig. 9. Depending on the direction of the eccentricity angle in the horizontal plane (left or right to the collimation axis) and the orientation of the measuring object (± IA), the measured D_{TLS} can be longer or shorter than the distance in the direction of the collimation axis (Fig. 9a). The eccentricity angle has a stronger effect on the D_{TLS} (ΔD_{ε}) with increasing IA (Fig. 9b). If the vertex of the eccentricity angle is not in the TLS + TS-zero point and is nearer to object, the influence of the same eccentricity angle is smaller and vice versa.

The eccentricity can occur in the horizontal and in the vertical direction. In view of the rotation of the measuring object about the approximately vertical axis during the investigation, only the horizontal component of the eccentricity is of importance. The eccentricity affects the measurements systematically and unilaterally and can change with the maintenance of the instrument.

Due to this influence, the D_{TLS} does not relate to measured Hz_{TLS}, V_{TLS}. This does not identify the corresponding D_{ref} for the distance comparison. The investigated distance deviations can thereby be biased.

2. Orientation unknown (influence on Hz_{TLS_ref}, V_{TLS_ref} of D_{TLS}, relevant for the 2[nd] and 3[rd] method)

If the *OU* used for the orientation of the TLS-point cloud in the reference CS system deviates from the true value, this deviation systematically affects the oriented Hz_{TLS_ref} ($Hz_{TLS\_ref} + \Delta OU$) corresponding to D_{TLS}. Thus, the D_{TLS} is not referring to the measuring object (Fig. 10a). This influence on the distances ΔD_{OU} has an effect with increasing IA (Fig. 10b).

3. Staking out at the distance of 30 m for the S-identification method (influence on D_{ref}, in the 1[st] method)

The accuracy of the aiming decreases as a result of the thickness of the crosshair and the magnification of the telescope, which essentially influences the signalizing of the scanned point by staking out. This influence is more apparent in the reference distance with increasing IA (standard deviation of a repeatedly staked out distance of 0.5 mm) and acts randomly on the reference determination.

4. TLS + TS-zero point determination (influence on D_{ref}, relevant for the 2[nd] and 3[rd] method)

If the estimation of the starting point of the D_{ref} is biased (Fig. 11a), the Hz_{ref} and Hz_{TLS_ref} do not have the same vertex. From this it follows that a parallel D_{ref} to D_{TLS} is found. Due to this influence, the reference distances are systematically corrupted by a constant part (ΔD_{P0c}) and an IA-dependent proportion (ΔD_{P0IA}, Fig. 11b). With regard to the research question treated here, particularly the second part has to be considered.

Table 2
Overview of methods and experiments.

Info	1st method	2nd method	3rd method
Measurement Acronym	e1.1 (e1.2)	e2.1	e3.1 (e3.2) (e3.3)
Time	10/2014 (03/2015)	10/2015	05/2016 (09/2016) (09/2016)
Instrument	MS50	maintained MS50	MS60 (MS50 new adjustment) (MS50)
Incidence angle [gon]	−(0, 10, 20, 30, 35, 40, 45, 50, 55, 60)		−(0, 10, 20, 30, 35, 40, 45, 50, 55, 60) ± (0, 10, 20, 30, 35, 40, 45, 50, 55, 60) ± (0, 10, 20, 30, 35, 40, 45, 50, 55, 60)
Reference instruments	Total Stations	Laser tracker, Scanner arm + triangulation scanner	Laser tracker + Close-range handheld laser scanner
Reference basis	High accuracy network (+reference scale)	High accuracy network	High accuracy network
Reference zero point	High accuracy network	Spatial backward intersection	Spatial backward intersection
Reference object point	Spatial forward intersection	Areawise triangulation, transformation – extern tie points - spheres	Areawise triangulation, transformation – intern tie points on the instrument (marker LED)
Orientation of TLS+TS point cloud in the reference CS	No	Yes	Yes
Identification Method	S-method	N-method	N-method

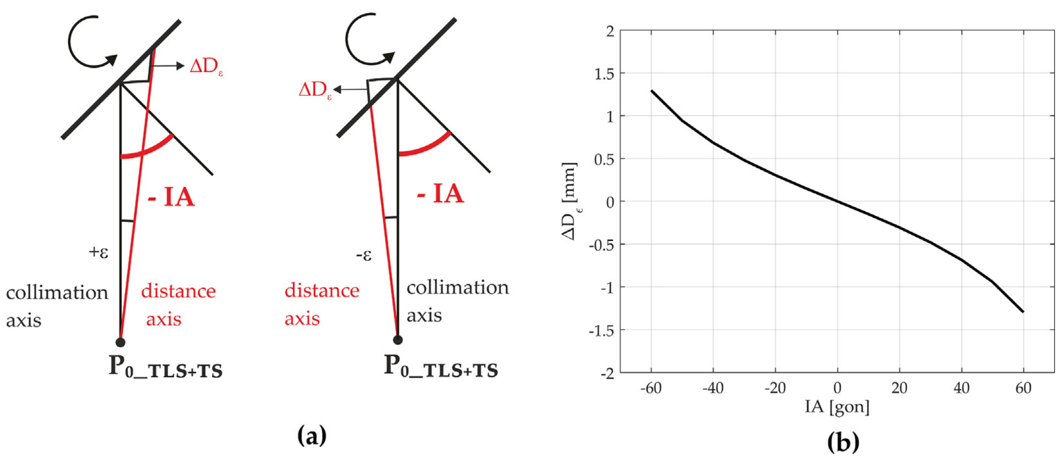

Fig. 9. Eccentricity between the collimation axis and the distance axis: (a) sketch; (b) simulation of this influence on the distance deviations under incidence angle ($\varepsilon = 2$ mgon, $D = 30$ m, vertex of the eccentricity angle = TLS + TS-zero point).

4.3. Correction of the influences

The mentioned influences can be handled in the following manner to minimize their effect on the observed distance deviations:

1. The aiming error and the staking out error cannot be reduced without a special solution (magnification of the telescope, thickness of the crosshairs) as the investigated distance of 30 m need to be kept constant.
2. The single correction of the eccentricity between the distance axis and the collimation axis is determined using the TS-part of the TLS + TS. The reflectorless distance is measured to a carefully targeted point in two faces several times under each IA. The mean value of the distances from both faces represents the correct distance D (Fig. 12). The eccentricity angle (ε) can be estimated from the differences (ΔD_e) between the correct distance and the distance in the first face D_{F1} under the IA

$$\Delta D_{\varepsilon} = D \cdot \left(\frac{1}{\cos(\varepsilon) - \tan(IA) \cdot \sin(\varepsilon)} - 1 \right). \tag{11}$$

In the first method, a distance correction corresponding to the estimated eccentricity angle can be applied to D_{TLS}, while in the second and third method, the eccentricity angle is applied to Hz_{TLS} used to identify the reference distances.

A disadvantage of the subsequent correction of the eccentricity is that its estimation is directly influenced by the standard deviations of the RL distance measurement, of the aiming and of the instability of the distance measurement.

3. A joint correction of the influences 1., 2., 4. in Section 4.2) is possible by the extension of the measuring process. The distance deviations are quantified under the same positive and negative IA (rotation of the object in the clockwise and counterclockwise directions) (Fig. 13).

By averaging the ΔD of the same positive and negative IA, these influences are eliminated (Fig. 13). The distance deviations and their standard deviations are expressed after correction for one IA

$$\Delta D = \frac{\Delta D_{m,+IA} + \Delta D_{m,-IA}}{2}, \tag{12}$$

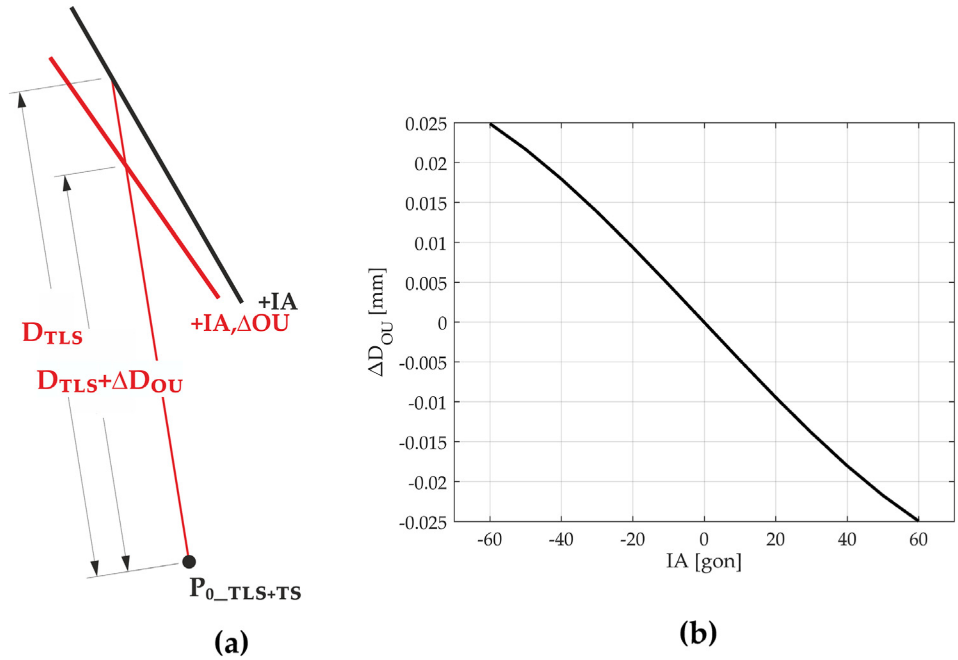

Fig. 10. Influence of the orientation unknown *OU* on the investigated distance deviation (a) sketch; (b) simulation of this influence on the distance deviations under incidence angle ($\Delta OU = -2$ mgon, $D = 30$ m).

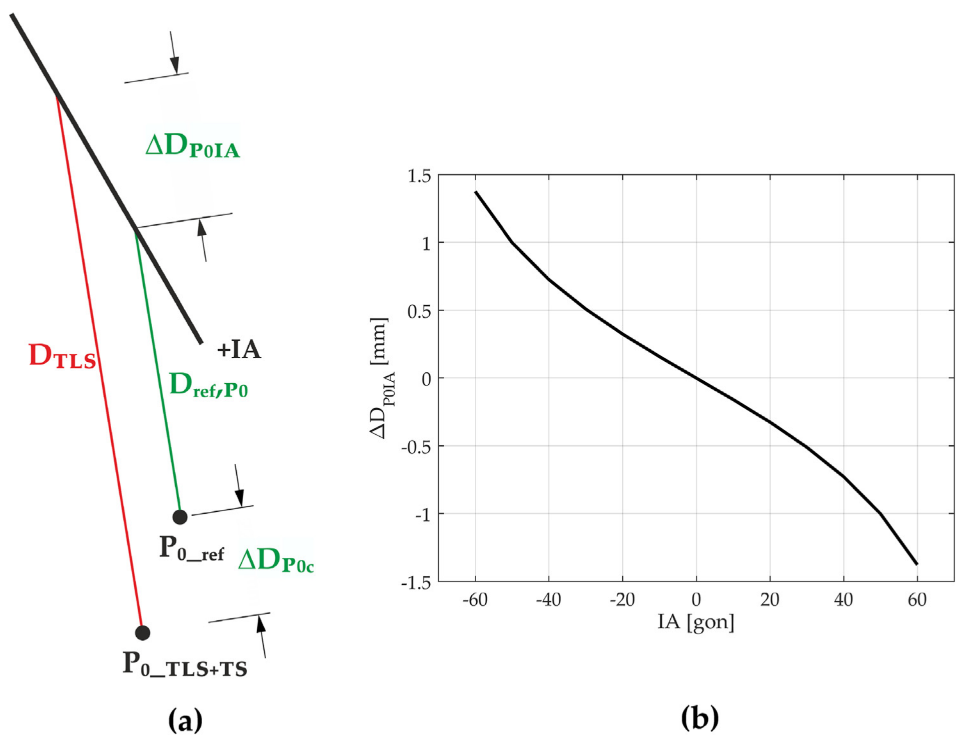

Fig. 11. Influence of the TLS + TS-zero point determination on the investigated distance deviation (a) sketch; (b) simulation of the IA-dependent portion of the influence on the distance deviations under incidence angle (normal distance from P_{0_ref} to D_{TLS} 1 mm, $D = 30$ m).

$$\sigma_{\Delta D} = \sqrt{\frac{\sigma_{\Delta Dm,+IA}{}^2 + \sigma_{\Delta Dm,-IA}{}^2}{4}}. \tag{13}$$

Table 3 confirms the applicability of the joint correction. For concrete realistic values of influences, the remaining influence after this correction causes a systematic distance deviation of 0.02 mm, which is sufficient for the investigation. The effect of the inequality between the positive and the negative *IA* on the elimination of influences is also mentioned.

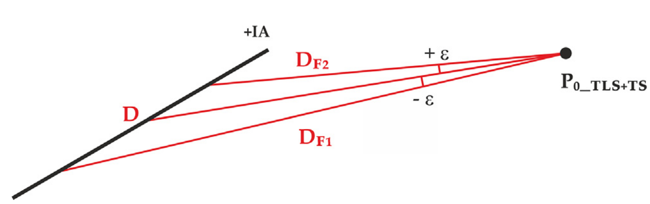

Fig. 12. Single correction of the eccentricity.

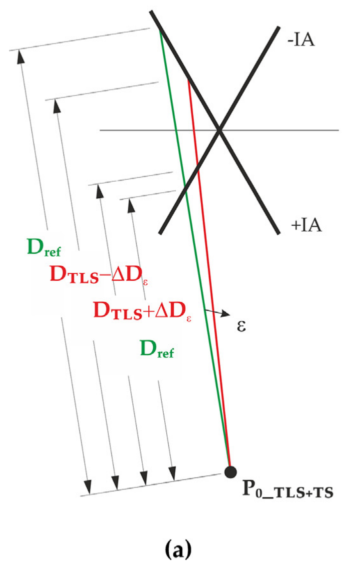

Fig. 13. Effect of the influences under positive and negative *IA*: (a) influence of the eccentricity between the distance axis and the collimation axis; (b) influence of the orientation unknown; (c) IA-dependent influence of the TLS + TS-zero point determination.

Table 3
Elimination of influences by corrections. Simulation for a point on the measuring object with a horizontal distance offset of 0.1 m from the vertical rotation axis, D = 30 m, ± IA = ± 60 gon. For joint correction, the difference between the same positive and negative IA is 1 gon.

Correction	Influence	Values	Remaining influence
Single correction of eccentricity	Eccentricity	Up to 0.02 gon	0.01 mm
Joint correction	Eccentricity (vertex of the eccentricity angle = TLS + TS-zero point)	Up to 2 mgon	0.01 mm
	Orientation-unknown	Up to 0.01 gon	0.01 mm
	Zero point determination – IA-dependent part	normal distance from P_{0_ref} to D_{TLS} 1 mm	0.02 mm

4.4. Raw and corrected results

The distance deviations ΔD_m obtained in all experiments are shown in Fig. 14 as a function of the IA. It can be noticed that the distance deviations curves are different. They are shifted at IA = 0 gon and in some cases the course is distinct.

The offset between the curves at IA = 0 gon occurs due to variations between the experiments. It is caused mainly by the determination of the station points in the first method and the TLS + TS-zero point determination in the second and third method, by aging (experiments over 2 years e1.1–e3.3) and maintenance of the instrument (before e2.1, before e3.2) and/or by the use of another instrument (at e3.1).

The different penetration of the laser beam is excluded as it is assumed that the laser beam of all instruments penetrates into the material in the same order of magnitude and the material is homogenous. Due to possible granite heterogeneity the transmission can influence more results of 1st method than 2nd and 3rd method because only a few distance deviations are averaged in the 1st method in comparison to 2nd and 3rd method where a few hundred of distance deviations were averaged. The mean value of the transmission effect can be included in

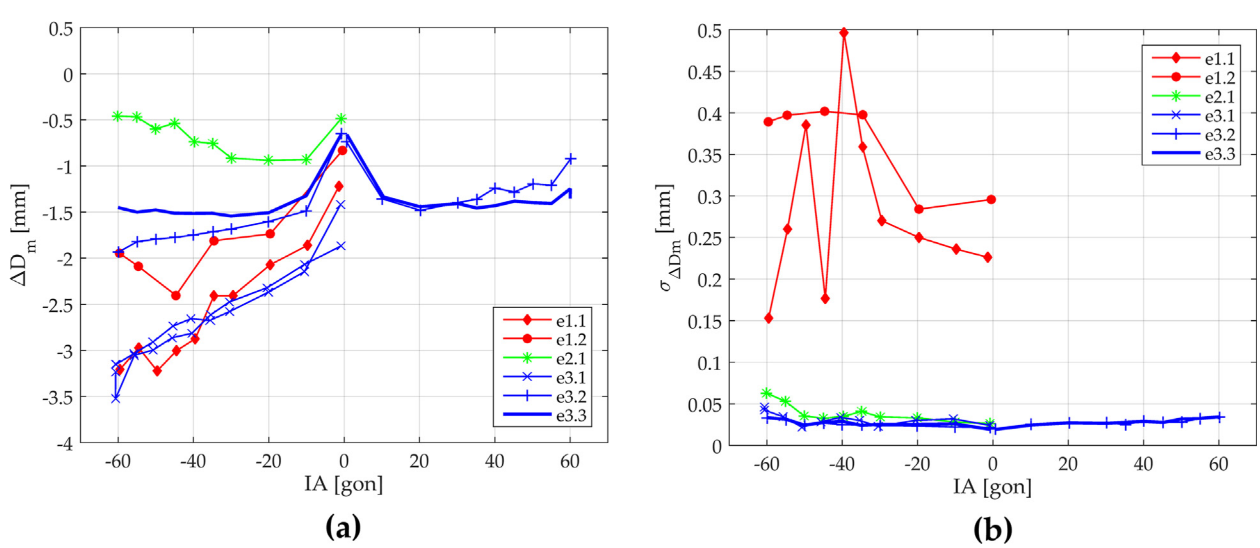

Fig. 14. (a) Quantified distance deviations under incidence angle in all of the experiments; (b) their standard deviations.

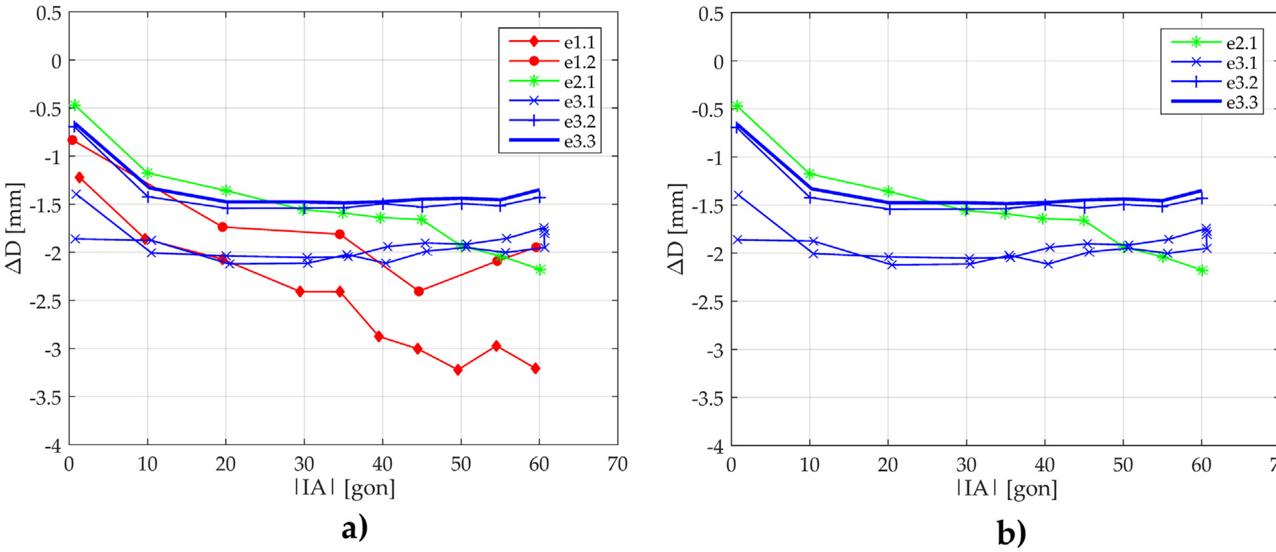

Fig. 15. Corrected distance deviations under incidence angle: (a) in all of the experiments; (b) in the last four experiments.

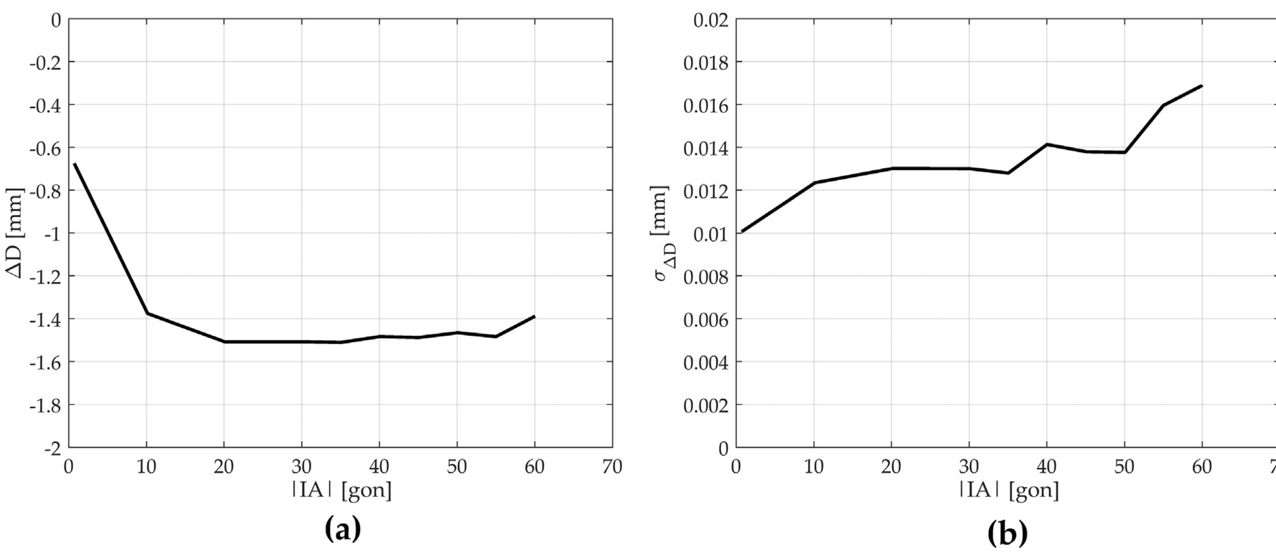

Fig. 16. (a) Final distance deviations under the incidence angle; (b) their standard deviations.

the results or directs to zero in dependence on material structure. This existing offset is not essential for the interested variation of the distance deviations over IA.

The differences between the courses of the ΔD with IA (Fig. 14a) can be caused by an individual influence or by a combination of the influences explained in Section 4.2: the staking out (e1.1, e1.2, zigzag course with higher IAs)), the eccentricity between the distance axis and the collimation axis (e1.1–e3.3), the orientation unknown (e2.1–e3.3) and the zero point determination (e2.1–e3.3).

In accordance to Section 4.3, the following corrections were applied to the raw results (Fig. 15). For the experiments e1.1–e3.1 only the eccentricity correction was applied in accordance to (11). Its determination in e1.1 and e1.2 was not accurately enough to quantify the influence in terms of a correction factor, which is clearly evident in the results. Additional investigations were conducted for the explanation. They indicated a large variation of the eccentricity after starting the instrument. As a result, sufficient warm-up of the instrument has to be ensured (recommendation - 3 h). However, this has not been sufficiently taken into account during e1.1 and e1.2. For e2.1 the eccentricity could not be completely eliminated due to its determination (see Section 4.3/2.), especially for higher *IA* (50–60 gon). In e3.2 and e3.3 the error influences due to the eccentricity, the orientation unknown and the zero point determination were corrected by the improved measuring setup via the measuring process and the following averaging of the ΔD_m for positive and negative *IA*. The corrected distance deviations obtained from these experiments is reliable, as the max. deviation between the curves is max. 0.09 mm.

4.5. Assessment of the influence of IA under framework condition

The influence of IA is observed by means of the results of e3.2 and 3.3, where possible error influences described in Section 4.2 are eliminated. The mean values of the corrected distance deviations for each IA from both experiments and their standard deviations are the input data for further analysis (Fig. 16).

As can be seen from Fig. 16 that when the laser beam falls perpendicular to the surface (IA = 0 gon), the D_{TLS} agrees best with the D_{ref}. Their difference amounts to 0.7 mm. This extension of the D_{TLS} indicates the penetration of the laser into material (Zámečníková et al., 2014b), the zero point error of the instrument or a combination of both.

The further course of the differences related to the IA is surprising (in accordance to Section 1). If the IA varies slightly from the perpendicular orientation to the object up to 20 gon, ΔD suddenly increases by 0.8 mm, from 20 gon to 60 gon ΔD reach relatively stable values with max. variation of 0.1 mm. Together, the ΔD vary in the range of 0.8 mm. The D_{TLS} are longer with the higher IA.

The distance variation under the influence of the IA was statistically assessed by Eqs. (5)–(7). The tested difference d_i between adjacent IA reaches values from −0.7 to 0.1 mm and its corresponding standard deviation is 0.02 mm. A significant variation of the D_{TLS} under IA up to 20 gon and between IA 55–60 gon was found. This also confirms a significant variation in the D_{TLS} between three intervals of IA – (0–20) gon, (20–55) and (55–60) gon.

5. Conclusion

In this paper, three methods that quantify systematic distance deviations under IA in scanning mode with scanning total stations were presented.

They solve the problem of the reproducibility of the scanned points, which always occurs in scanning. The methods are based on the direct comparison of the reference distance D_{ref} with the D_{TLS}. The reference distance is derived in three parts of the reference measurement: 1. high accuracy network measurement, 2. TLS + TS-zero point measurement, 3. object point measurement. In the first method, the first two parts are connected.

The assignment of the D_{TLS} to the D_{ref} in the first method is realized by the Hz-, V-staking out of a single endpoint (S-method). In the second and third method, the corresponding D_{ref} is searched in a dense reference scan using Hz_{TLS}, V_{TLS} under conditions that D_{ref} and D_{TLS} are oriented with respect to the same reference CS (N-method). In the S-method, the TLS-point cloud remains in the instrument TLS + TS CS. In contrast, in the N-method the orientation of the TLS-point cloud with respect to the reference CS is necessary. This method allows the determination of several distance deviations – some hundreds per one alignment of the measured object. Opposite to that the S-method is restricted from practical point of view to few points (1–10). Nevertheless, the N-method is much faster.

The first method uses three total stations (two of them are of the highest accuracy) and a reference scale. In the second method, a laser tracker and a scanner arm with a triangulation scanner are used. The third method implements a laser tracker linked to a close range handheld scanner.

The most important influences on the reference determination in the first method are aiming and staking out of the endpoints of the examined distances D_{TLS}. In the second method, the transformation of the reference point cloud is essentially. In all methods, the influence of the eccentricity between the collimation axis and the distance axis has to be eliminated. A viable solution is the averaging of the determined distance deviations under the same negative and positive IA.

The uncertainty of the presented methods i.e. of D_{ref} (averaged over one object alignment) is from 0.1 to 0.3 mm. The higher uncertainty of 0.3 mm at 30 m reaches the second and first method where the staking out limits the achievable uncertainty. An uncertainty of 0.1 mm was obtained in the third method.

The time required for the network measurement and the zero point determination in all methods is approximately two hours (pure measurement without setup). The main difference between the methods addresses the object measurement. In the first method (TLS-scan, staking out, TMS measurement) the measurements in one alignment of the measured object (1 IA) require 30 min. A significant time saving is achieved in the second method. For a TLS-scan and the measurement of the tie points with LT only 2 min are necessary. One reference scan and the measurement of the tie points of the object are recorded with SA, in 30 min. The third method (TLS-scan and reference scan with the handheld scanner) requires 4 min.

These methods were validated with the scanning total station MS50 under comparison conditions. A granite plate was rotated with respect to the vertical axis and measured at a distance of 30 m.

The results exhibit influences of measuring process and of instrumental errors increasing with IA. These influences need to be eliminated. The last two experiments in the third method point to a fully developed method. The maximum difference between the two obtained results is of 0.09 mm. Under IA of 0–60 gon the D_{TLS} vary in the interval of 0.8 mm. These values are not transferable to other materials and they refer only to defined framework conditions.

A comprehensive assessment of the influence of the IA on the distance measurement of scanning total stations still requires further investigations e.g. under varying distances, different materials, and roughness levels. It is also important to consider the interplay of these factors with different TLS + TS, the other parameters of the laser and the distance measurement. These influences can lead to a variation of the systematic distance deviations which differs from the one presented in this paper.

The introduced methods provide a useful basis for future studies of the mentioned influences as well as their interplay. They allow the further analysis of the variation of diverse influences under IA on the distance measurement, e.g. transmission, roughness.

One further task addressed in future works will concern the adaption of the third method to conventional TLS. If the zero point determination is adapted for TLS by replacing the CCR reflector with TLS-targets, the method should be applicable.

Acknowledgments

We sincerely thank Mr. Stefan Horvath (Hexagon Metrology GmbH) for providing the necessary measuring equipment to produce the reference distances. We thank Mr. Florian Rist, Mrs. Dragana Panic, Mr. Stefan Pegritz, Mr. Robert Sonnleitner for their valuable help during the measurements.

This research did not receive any specific grant from funding agencies in the public, commercial, or not-for-profit sectors.

Appendix A

See Tables A1 and A2.

Table A1
Uncertainty budget of reference distance of the first method.

Part	Influence		Parameter/Action	Value
High accuracy network, starting point	Point signalizing	Prisms	Centering error, remaining prisms in tribraches	
		Instruments	Centering error, remaining instruments in tribraches	
		Stability of station points during measurement	Max. *Hz*-deviation from the sum of the interior angles of the triangle (TLS + TS, TS_1, TS_2)	1.2 mgon
			Max. difference in *Hz*, *V* between station points	0.9 mgon
			Max. difference in *Hz*, *V* of station points to prisms	1.4 mgon
			Max. difference of basis TS_1,TS_2	0.12 mm
	Angle measurement	Axis errors	Influence eliminated in two faces	
	Distance measurement	Zero point error	Considered	
		Scale factor	Basis determination by Hansen's task	
		Atmospheric correction	Considered	
	Leveling	Skewness of the trunnion axis	Setting accuracy of compensator of 0.15 mgon → max. impact on the angle measurement to network points (V = 83–102 gon), adjustment of three station points	
	Point accuracy	Network adjustment	Max. coordinate standard deviation of prisms	0.10 mm
			Max. coordinate standard deviation of station points	0.05 mm
Signalizing of the endpoint	*Hz*, *V*- accuracy	Manufacturer	Angle measurement standard deviation of 0.3 mgon → max. impact on the distance under IA = 60 gon	0.4 mm
	Hz, *V*-driving of the scanned point	Driving accuracy	Max. *Hz*-deviation of the scanned point	0.6 mgon
			Max. impact on the distance under IA = 60 gon	0.4 mm
	Eccentricity between the distance and the collimation axis	Measurement with TS-part of TLS + TS	Distance measurement to one point in two faces 15x:	
			Mean of the distance deviations	0.04 mm
			Empirical standard deviation	0.15 mm
	Repeatability of the staked out distance	TMS-determination	1 point under IA = 55 gon 12x staked out and determined by TMS → distance standard deviation	0.25 mm
			Double determination of distances to 5 points under IA 0, 40, 45, 55, 60 gon → distance standard deviation	0.05–0.51 mm
	Stability of the measuring object	TMS-measurement of 4 control points before and after the staking out	Max. coordinate deviation	0.05 mm
Determination of the endpoint	Angle measurement	Error influences	As in the network	
		Skewness of the trunnion axis	Setting accuracy of compensator of 0.15 mgon → max. impact on the angle measurement to object points (V = 111–116 gon, D = 2 m)	0.04 mgon
		Twisting of the *Hz*-circle at TS_1, TS_2	Check – mutual collimation before object measurement under each IA	
	Azimuth accuracy at TS_1, TS_2	Error propagation law	Azimuth standard deviation	1.2 mgon
	Basis accuracy TS_1, TS_2	Error propagation law	Basis standard deviation	0.02 mm
	Repeatability of the distance to the endpoint	TMS-measurement	1 point measured 12x → distance standard deviation	0.01 mm

Table A2
Uncertainty of reference distance of the first method (IA = 60 gon).

Input quantity	Estimated value [m]	Standard uncertainty	Distribution assumption	Uncertainty amount	Type of the component
Y_{ref_P0}	0.00007	0.001 mm	Normal		A, Adjustment
X_{ref_P0}	-0.00026	0.05 mm	Normal		A, Adjustment
Z_{ref_P0}	0.00013	0.02 mm	Normal		A, Adjustment
Y_{ref_Pi}	0.03096	0.01 mm	Normal		A, Error propagation law
X_{ref_Pi}	29.98078	0.02 mm	Normal		A, EPL
Z_{ref_Pi}	-0.32253	0.01 mm	Normal		A, EPL
Scanning (Hz_{TLS}, V_{TLS})	0	0.3 mgon (0.13 mgon)	Normal	0.19 mm (0.08 mm)	B, Manufacturer
Driving (Hz_{TLS}, V_{TLS})	0	0.3 mgon (0.13 mgon)	Normal	0.19 mm (0.08 mm)	B, Manufacturer
Staking out	0	0.50 mm (0.22 mm)	Normal	0.5 mm (0.22 mm)	B, Manufacturer
Eccentricity	0		Normal		B, Investigation

Uncertainty of D_{ref} (mean value of 5 $D_{ref)}$ = 0.25 mm.

Appendix B

See Tables B1 and B2.

Table B1
Uncertainty budget of the reference distance of the second method.

Part	Influence		Parameter/Action	Value
High accuracy network	Point signalizing	CCR-reflector	Centering error	< 0.003 mm
	Angle measurement	Axis errors	Eliminated in two faces	
	Distance measurement	Atmospheric correction	Considered	
		Distance noise	Reduced with measurement time of 5 s	
	Leveling	Inclination measurement	MPE at $D = 10$ m	0.09 mm
	Measurement repeatability	Repeated putting the reflector in the nest	Max. coordinate difference	0.03 mm
	Point accuracy	Network adjustment	Max. coordinate standard deviation	0.08 mm
Starting point	Angle measurement	Axis errors	Eliminated in two faces	
		Skewness of the trunnion axis	Setting accuracy of compensator of 0.15 mgon → max. impact on the angle measurement to network points (V = 90.93–100.74 gon, max. $D = 6$ m)	0.02 mgon
	TLS + TS-stability (P_0)	Measurement to network points	Max. difference between Hz, V at the beginning and at the end (lateral deviation)	1.5 mgon (0.07 mm)
		P_0 – new determination	Max. coordinate difference at the beginning and at the end	0.05 mm
	P_0-accuracy	Adjustment	Max. coordinate standard deviation	0.02 mm
	Network inclination	Simulation	MPE of inclination measurement at $D = 26$ m, i.e. 0.55 mgon →	
			Max. impact on Z-coordinate of the zero point	0.18 mm
			Max. impact on the Y, X-coordinates of the zero point	0.00 mm
Endpoint	LT-stability	Measurement to network points	Max. coordinate difference at $D = 23$ m	0.10 mm
	SA-accuracy	Measurement of tie points and object scanning	2 standard deviation	0.016 mm
	LT-accuracy	Tie points measurement	MPE of a coordinate at $D = 8$ m	0.06 mm
	Transformation of the reference point cloud	Tie points measured by SA and LT	Max. residual of a coordinate	0.10 mm
Spatial assignment $D_{TLS\_i} - D_{ref\_i}$	Orientation of TLS-point cloud	Orientation unknown	Empirical standard deviation of mean value	0.08 mgon
			Starting point – see above	
			Hz_{ref} to network points – skewness of LT-trunnion axis	0.00 mgon
			Hz_{TS} to network points – skewness of TLS + TS-trunnion axis; setting accuracy of compensator of 0.15 mgon → max. impact on the angle measurement to network points (V = 90.93–100.74 gon, max. $D = 6$ m)	0.02 mgon
	Horizontal CS	LT-CS, inclination measurement	MPE of inclination measurement → max. impact on the Hz-direction of LT_2 - Hz_{zref} to object points (V = 99.82–104.34 gon, D = 8 m)	0.04 mgon
		TLS + TS-CS, compensator	Setting accuracy of compensator of 0.15 mgon → max. impact on the angle measurement to object points (V = 99.86–100.29 gon, $D = 30$ m)	0.00 mgon
	Eccentricity between the distance axis and the collimation axis at TLS + TS	Horizontal	Additional investigation – distance measurement in two faces by TS-part of TLS + TS, estimation	2.81 mgon
		Vertical	Low effect due to the rotation of the measuring object about a nearly vertical axis	
	Threshold values	Due to IA	Max. impact under $IA = 60$ gon	0.06 mm
	ΔHz, $\Delta V = 0.1$ mgon,	Due to roughness	Reduced by averaging the ΔD over a alignment of the measuring object	
	Hz_{TLS}, V_{TLS}-noise		Reduced by averaging the ΔD over a alignment of the measuring object	

Table B2
Uncertainty of the reference distance of the second method (IA = 60 gon).

Input quantity	Estimated value [m]	Standard uncertainty	Distribution assumption	Type of the component
Y_{ref_P0}	−6.94582	0.02 mm	Normal	A, Adjustment
X_{ref_P0}	21.13563	0.02 mm	Normal	A, Adjustment
Z_{ref_P0}	−0.20282	0.09 mm	Normal	B, Simulation
Y_{ref_Pi}	4.78752	0.25 mm	Normal	A, Adjustment
X_{ref_Pi}	−6.22431	0.31 mm	Normal	A, Adjustment
Z_{ref_Pi}	−0.24628	0.37 mm	Normal	A, Adjustment
ΔHz, ΔV	0	0.06 mm	Normal	B, Precalculation

Uncertainty of D_{ref} = 0.30 mm.

Appendix C

See Tables C1 and C2.

Table C1
Uncertainty budget of the reference distance of the third method.

Part	Influence		Parameter/Action	Value
High accuracy network	Point signalizing	CCR-Reflector	Centering error	< 0.003 mm
		Point stability, transformation of the network at the beginning and the end	Max. coordinate deviation	0.04 mm
	Angle measurement	Axis errors	Eliminated in two faces	
	Distance measurement	Atmospheric correction	Considered	
		Distance noise	Reduced with measurement time of 5 s	
	Leveling	Inclination measurement	MPE at D = 10 m	0.09 mm
	Measurement repeatability	Repeated putting the reflector in the nest	Max. coordinate difference	0.03 mm
	Point accuracy	Network adjustment	Max. coordinate standard deviation	0.06 mm
Starting point	Angle measurement	Axis errors	Eliminated in two faces	
		Skewness of the trunnion axis	Setting accuracy of compensator of 0.15 mgon → max. impact on the angle measurement to network points (V = 81.57–114.80gon, max. D = 6 m)	0.05 mgon
	TLS + TS-stability (P_0)	Measurement to network points	Max. difference between Hz, V at the beginning and at the end (lateral deviation)	0.6 mgon (0.05 mm)
		P_0 – new determination	Max. coordinate difference at the beginning and at the end	0.03 mm
	P_0-accuracy	Adjustment	Max. coordinate standard deviation	0.02 mm
	Network inclination	Simulation	MPE of inclination measurement at D = 20 m, i.e. 0.56 mgon:	
			Max. impact on Z-coordinate of the zero point	0.12 mm
			Max. impact on the Y, X-coordinates of the zero point	0.01 mm
Endpoint	LT-stability for HS	Measurement to network points	Max. coordinate difference	0.05 mm
	HS-accuracy	Manufacturer	MPE of a coordinate	0.06 mm
Spatial assignment $D_{TLS\_i} - D_{ref\_i}$	Orientation of TLS-point cloud	Orientation unknown	Empirical standard deviation of mean value	0.07 mgon
			Starting point – see above	
			Hz_{ref} to network points – skewness of LT-trunnion axis	0.00 gon
			Hz_{TS} to network points – skewness of TLS + TS-trunnion axis, setting accuracy of compensator of 0.15 mgon → max. impact on the angle measurement to network points (V = 81.57–114.80 gon, max. D = 6 m)	0.05 mgon
	Horizontal CS	LT-CS, inclination measurement	MPE of inclination measurement → max. impact on the Hz-direction Hz_{ref} to object points (V = 100.59-101.51 gon, D = 16.5 m))	0.01 mgon
		TLS + TS-CS, compensator	Setting accuracy of compensator of 0.15 mgon → max. impact on the angle measurement to object points (V = 99.91–100.33 gon, D = 30 m)	0.00 mgon
	Eccentricity between the distance axis and the collimation axis at TLS + TS	Horizontal	Eliminated by averaging of ΔD under the same positive and negative IA	
		Vertical	Low effect due to the rotation of the measuring object about a nearly vertical axis	
	Threshold values	Due to IA	Max. impact under IA = 60 gon	0.06 mm
	ΔHz, ΔV = 0.1 mgon,	Due to roughness	Reduced by averaging the ΔD over a alignment of the measuring object	
	Hz_{TLS}, V_{TLS}-noise		Reduced by averaging the ΔD over a alignment of the measuring object	

Table C2
Uncertainty of the reference distance of the third method (IA = 60 gon).

Input quantity	Estimated value [m]	Standard uncertainty	Distribution assumption	Type of the component
Y_{ref_P0}	−13.58751	0.02 mm	Normal	A, Adjustment
X_{ref_P0}	0.19628	0.02 mm	Normal	A, Adjustment
Z_{ref_P0}	−0.21562	0.06 mm	Normal	B, Simulation
Y_{ref_Pi}	16.33504	0.06 mm	Normal	B, Manufacturer
X_{ref_Pi}	−1.37409	0.06 mm	Normal	B, Manufacturer
Z_{ref_Pi}	−0.24628	0.06 mm	Normal	B, Manufacturer
ΔHz, ΔV	0	0.06 mm	Normal	B, Precalculation

Uncertainty of D_{ref} = 0.09 mm.

References

Agilent Technologies, 2008. Agilent 5530 Dynamic Calibrator. Measurement Reference Guide. Agilent Technologies.

Boehler, W., Marbs., 2008. Investigating laser scanner accuracy. In: The International Archives of Photogrammetry, Remote Sensing and Spatial Information Sciences, 34. Available online: < https://hds.leica-geosystems.com/hds/en/Investigating_Acurracy_Mintz_White_Paper.pdf > (accessed on 25.06.2018).

Dorninger, P., Nothegger, C., Pfeifer, N., Molnár, G., 2008. On-the job detection and correction of systematic cyclic distance measurement errors of terrestrial laser scanners. J. Appl. Geodesy 2, 191–204. https://doi.org/10.1515/JAG.2008.022.

Eling, D., 2009. Terrestrisches Laserscanning für die Bauwerksüberwachung. PhD thesis. Leibniz Universität, Hannover.

Ge, X., 2016. Terrestrial laser scanning technology from calibration to registration with respect to deformation monitoring. PhD thesis. TU München.

Geotech. Leica TPS1200 Series, 2006. Available online: < http://www.geotech.sk/OLD/t7_TPS1200en.pdf > (accessed on 02.04.2018).

Gordon, B., 2008. Zur Bestimmung von Messunsicherheiten terrestrischer Laserscanner. PhD thesis. TU Darmstadt.

Heunecke, O., Kuhlmann, H., Welsch, W., Eichhorn, A., Neuner, H., 2013. Auswertung geodätischer Überwachungsmessungen, second ed. Wichmann Verlag, Berlin, Germany.

Hexagon Manufacturing Intelligence, 2015. Leica Absolute Tracker AT960 Brochure. Available online: < http://www.hexagonmi.com/products/laser-tracker-systems/leica-absolute-tracker-at960 > (accessed on 22.01.2018).

Hexagon Manufacturing Intelligence, 2018. Leica Absolute Scanner LAS-20-8, 2018. Available online: < http://www.hexagonmi.com/products/3d-laser-scanners/leica-absolute-scanner-las-20-8 > (accessed on 22.01.2018).

Holst, Ch., Kuhlmann, H., 2014. Aiming at self-calibration of terrestrial laser scanners using only one single object and one single scan. J. Appl. Geodesy 8 (4), 295–310. https://doi.org/10.1515/jag-2014-0017.

ISO17123-4, 2012. Optics and optical instruments – Field procedures for testing geodetic and surveying instruments – Part 4: Electro-optical distance meters (EDM measurements to reflectors).

JCGM 100:2008. Evaluation of measurement data—Guide to the expression of uncertainty in measurement, 2008. Available online: < https://www.bipm.org/utils/common/documents/jcgm/JCGM_100_2008_E.pdf > (accessed on 02.04.2018).

Joeckel, R., Stober, M., Huep, W., 2008. Elektronische Entfernungs- und Richtungsmessung und ihre Integration in aktuelle Positionierungsverfahren, fifth ed. Wichmann Verlag, Heidelberg, Germany.

Jutzi, B., 2007. Analyse der zeitlichen Signalform von rückgestreuten Laserpulsen. PhD thesis. TU München.

Kahmen, H., 2006. Angewandte Geodäsie: Vermessungskunde, 20nd ed. Walter de Gruyter Verlag, Berlin, Germany.

Kern, F., 2003. Automatisierte Modellierung von Bauwerksgeometrien aus 3D-Laserscanner-Daten. PhD thesis. Geodätische Schriftenreihe der Technischen Universität Braunschweig.

Kersten, T., Mechelke, K., Lindstaedt, M., Sternberg, H., 2008. Geometric accuracy investigations of the latest terrestrial laser scanning systems. In: FIG Working Week, Stockholm. Available online: < http://www.fig.net/resources/proceedings/fig_proceedings/fig2008/papers/ts02d/ts02d_01_mechelke_etal_2785.pdf > (accessed on 22.01.2018).

Leica Geosystems, 2009a. Leica TM30 Technical Data. Available online: < http://hds.leica-geosystems.com/downloads123/zz/tps/TM30/brochures-datasheet/TM30_Technical_Data_en.pdf > (accessed on 02.04.2018).

Leica Geosystems, 2009b. Leica TPS1200+ Series. Technical Data. Available online: < http://hds.leica-geosystems.com/downloads123/zz/tps/tps1200/brochures-datasheet/Leica_TPS1200+_TechnicalData_en.pdf > (accessed on 02.04.2018).

Leica Geosystems, 2015. MS60/TS60 User Manual.

Lichti, D.D., 2007. Error modelling, calibration and analysis of an AMCW terrestrial laser scanner system. ISPRS J. Photogramm. Remote Sens. 61, 307–324. https://doi.org/10.1016/j.isprsjprs.2006.10.004.

Lichti, D.D., Chow, J., Lahamy, H., 2011. Parameter de-correlation and model-identification in hybrid-style terrestrial laser scanner self-calibration. ISPRS J. Photogramm. Remote Sens. 66 (3), 317–326. https://doi.org/10.1016/j.isprsjprs.2010.12.001.

Lindstaedt, M., Kersten, T., Mechelke, K., Graeger, T., Sternberg, H., 2009. Phasen im Vergleich – Erste Untersuchungsergebnisse der Phasenvergleichsscanner FARO Photon und Trimble GX. In: Photogrammetrie, Laserscanning, Optische 3D-Messtechnik – Beiträge der Oldenburger 3D-Tage 2009, 1st ed. Wichmann Verlag, Heidelberg, Germany, pp. 53–64.

Mathworks, 2017. Geodetic Transformations. Available online: < https://de.mathworks.com/matlabcentral/fileexchange/9696-geodetic-transformations > (accessed on 22.01.2018).

Mechelke, K., Kersten, T., Lindstaedt, M., 2007. Comparative investigation into the accuracy behaviour of the new generation of terrestrial laser scanning systems. In: Optical 3-D Measurement Techniques VIII, Zürich, pp. 319–327.

Niemeier, W., 2008. Ausgleichungsrechnung, second ed. Walter de Gruyter, Berlin, Germany.

Reshetyuk, Y., 2009. Self-calibration and direct georeferencing in terrestrial laser scanning. PhD thesis. KTH Royal Institute of Technology.

Roncat, A., 2014. Backscatter signal analysis of small-footprint full-waveform lidar data. PhD thesis. TU Wien.

Sarti, P., Vittuari, L., Abbondanza, C., 2009. Laser scanner and terrestrial surveying applied to gravitational deformation monitoring of large VLBI telescopes' primary reflector. J. Surv. Eng. 139 (4), 136–148.

Schäfer, T., 2017. Berührungslose und flächenhafte Deformationsmessungen an Betonoberflächen unter besonderer Berücksichtigung der Interaktion zwischen Laserstrahl und Oberfläche. PhD thesis. TU München.

Schäfer, T., Schulz, T., 2005. Kalibrierung, Einflussgrößen und Genauigkeiten von Terrestrischen Laserscannern. In: Terrestrisches Laserscanning (TLS), Schriftenreihe des DVW. Wißner Verlag, Augsburg, Germany, pp. 29–48.

Schulz, T., 2007. Calibration of a terrestrial laser scanner for engineering geodesy. PhD thesis. ETH Zürich.

Soudarissanane, S., Lindenbergh, R., Menenti, M., Teunissen, P., 2011. Scanning geometry: influencing factor on the quality of terrestrial laser scanning points. ISPRS J. Photogramm. Remote Sens. 66 (4), 389–399. https://doi.org/10.1016/j.isprsjprs.2011.01.005.

SouVR, 2017. Metris Model Maker Scanners MMD/MMC. Available online: < http://en.souvr.com/product/200905/1919.html > (accessed on 16.03.2017).

Surveyequipment, 2013. Leica MS50/TS50/TM50 User Manual. Available online: < http://surveyequipment.com/assets/index/download/id/219/ > (accessed on 22.01.2018).

Thorlabs, 2018. Aluminum Breadboards. Available online: < https://www.thorlabs.com/newgrouppage9.cfm?objectgroup_id=1877 > (accessed on 02.04.2018).

Wang, J., 2013. Towards deformation monitoring with terrestrial laser scanning based on external calibration and feature matching methods. PhD thesis. Leibniz Universität Hannover.

Wujanz, D., Burger, M., Mettenleiter, M., Neitzel, F., 2017. An intensity-based stochastic model for terrestrial laser scanners. J. Photogram. Remote Sens. 125, 146–155.

Zámečníková, M., Neuner, H., Pegritz, S., 2014a, Influence of the incidence angle on the reflectorless distance measurement in close range. In: Ingeo 2014, 6th International Conference on Engineering Surveying, Prag. Available online: < https://www.fig.net/resources/proceedings/2014/2014_ingeo/TS8-01_Zamecnikova.pdf.pdf > (accessed on 22.01.2018).

Zámečníková, M., Neuner, H., 2017a. Untersuchung des gemeinsamen Einflusses des Auftreffwinkels und der Oberflächenrauheit auf die reflektorlose Distanzmessung beim Scanning. In: Lienhart, W. (Ed.), Ingenieurvermessung 17. Beiträge zum 18. Internationalen Ingenieurvermessungskurs Graz. Wichmann Verlag, Berlin/Offenbach, Germany, pp. 63–76.

Zámečníková, M., Neuner, H., 2017b. Investigation of the distance dependence of the combined influence of the incidence angle and the surface roughness on the reflectorless distance measurement of a scanning total station. Allgemeine Vermessungsnachrichten 11–12, 553–561.

Zámečníková, M., Wieser, A., Woschitz, H., Ressl, C., 2014b. Influence of surface reflectivity on reflectorless electronic distance measurement and terrestrial laser scanning. J. Appl. Geodesy 8 (4), 311–325. https://doi.org/10.1515/jag-2014-0016.

Zámečníková, M., Neuner, H., Pegritz, S., Sonnleitner, R., 2015. Investigation on the influence of the incidence angle on the reflectorless distance measurement of a terrestrial laser scanner. Österreichische Zeitschrift für Vermessung und Geoinformation (VGI) 103 (2+3), 208–218.

Zogg, H., 2008. Investigations of high precision terrestrial laser scanning with emphasis on the development of a robust close-range 3D-laser scanning system. PhD thesis. ETH Zürich.